Supplementary Information

In-Situ Growth of Porphyrinic Metal-Organic Framework Nanocrystals on Graphene Nanoribbons for Electrocatalytic Oxidation of Nitrite

Chung-Wei Kung,[a] Yan-Sheng Li,[b] Min-Han Lee,[a] Shan-Yu Wang,[b] Wei-Hung Chiang[b] and Kuo-Chuan Ho[a,c]**

[a] Department of Chemical Engineering, National Taiwan University, Taipei 10617, Taiwan

[b] Department of Chemical Engineering, National Taiwan University of Science and Technology, Taipei 10617, Taiwan

[c] Institute of Polymer Science and Engineering, National Taiwan University, Taipei 10617, Taiwan

S1. Synthesis of SWCNTs

The SWCNTs used in the present study were synthesized using a water-assisted catalytic chemical vapor deposition (CVD). In brief, Fe films (1.5 nm thickness) and an alumina (Al_2O_3) support layer (40 nm thickness) sputtered onto 1 cm × 1 cm polished silicon (Si) substrates with a silicon dioxide (SiO_2) layer of 600 nm were used as the catalyst films for CNT growth. The CNT were synthesized at one atmospheric pressure in a 3 inch quartz tube furnace with two process steps, including catalyst particle formation and CNT growth. For a typical catalyst particle formation experiment, we first flowed 200 sccm (sccm denotes standard cubic centimeter per minute at 1 atm) helium (He) and 1800 sccm hydrogen (H_2) for 15 minutes while ramping the temperature from room temperature to 810 °C, then keep same gas flow rates for 15 minutes to anneal the catalyst particles. Then CNT growth began for 10 minutes using a water-assisted CVD process at 810 °C with the gas mixture of 100 sccm ethylene (C_2H_4) and 900 sccm H_2, and 100 ppm water vapor as the carbon precursor and the catalyst preserver and enhancer, respectively. Water vapor of 100

ppm was supplied by passing 1000 sccm He carrier gas through a water bubbler with deionized (DI) water at STP (STP denotes standard condition for temperature and pressure, NIST version) condition. Water vapor concentration was monitored by a single-channel moisture meter (General Electric, MMS 35-211-1-100) coupled with a moisture probe (General Electric, M2LR) installed before the CVD reactor. All gas flows were controlled by mass flow controllers that were carefully calibrated before experiments to precisely control the gas concentrations in the CVD reactor.

S2. Photos of the as-prepared thin films

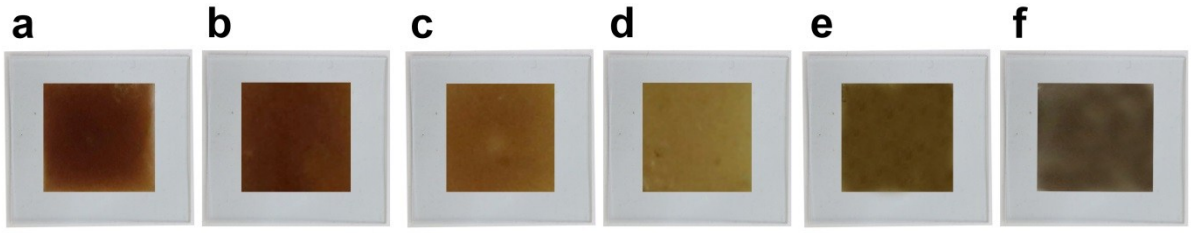

Figure S1. Photos of the obtained thin films of a) **MOF-525** nanocrystals, b) MOF-GNRs-5, c) MOF-GNRs-10, d) MOF-GNRs-25, e) MOF-GNRs-50, and f) GNRs on ITO substrates.

S3. Low-magnification and mid-magnification SEM images

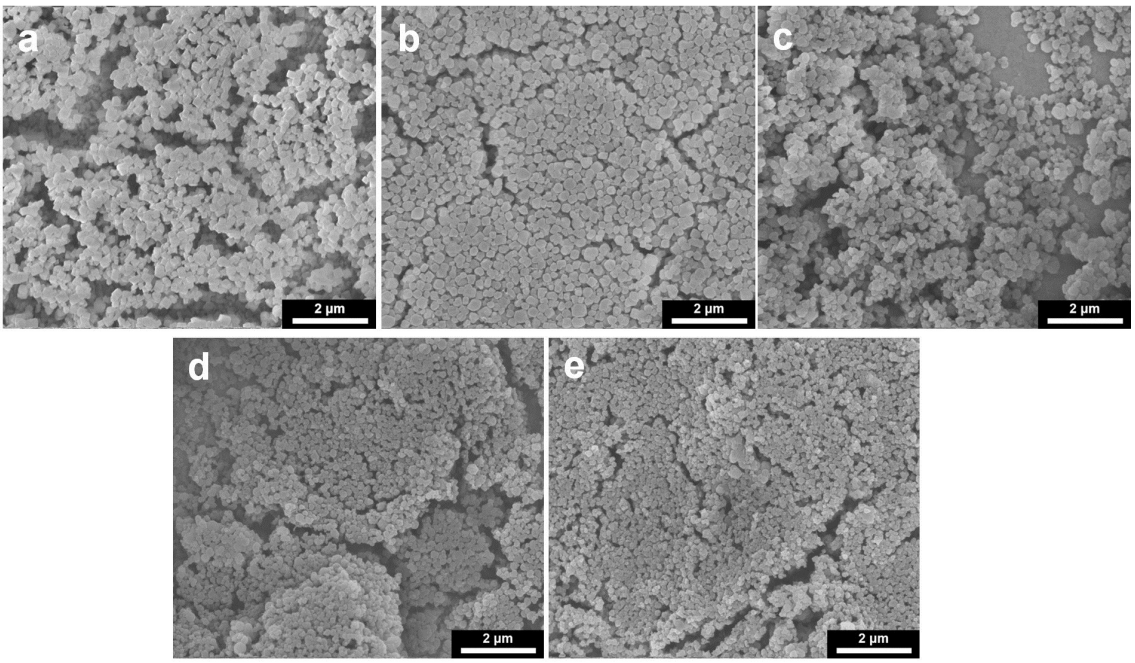

Figure S2. Low-magnification SEM images of a) **MOF-525** nanocrystals, b) MOF-GNRs-5, c) MOF-GNRs-10, d) MOF-GNRs-25, and e) MOF-GNRs-50.

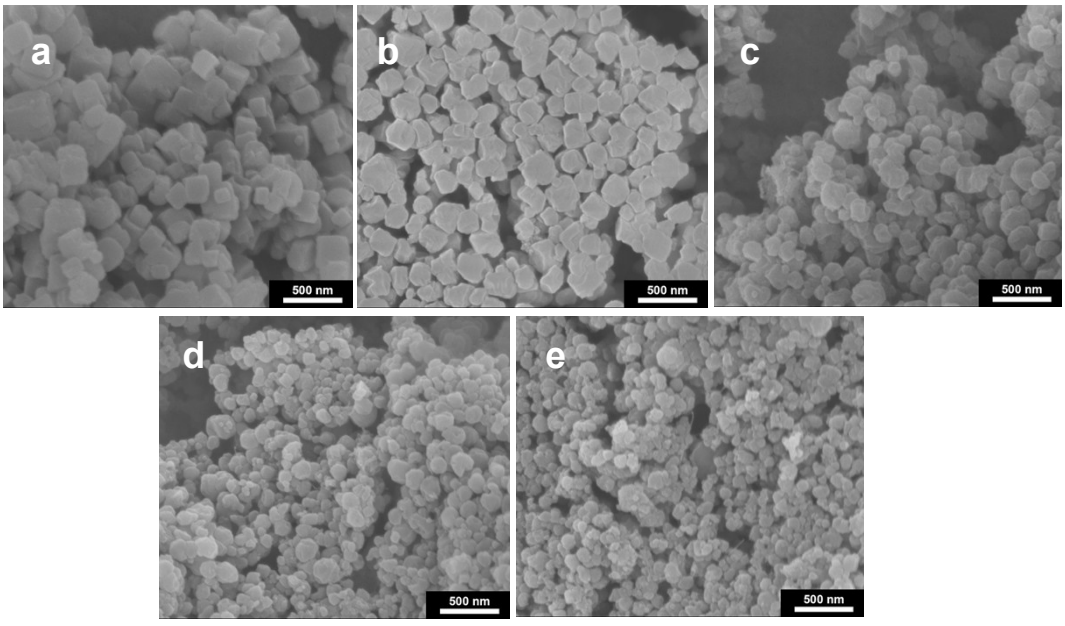

Figure S3. Mid-magnification SEM images of a) **MOF-525** nanocrystals, b) MOF-GNRs-5, c) MOF-GNRs-10, d) MOF-GNRs-25, and e) MOF-GNRs-50.

Table S1. Evaluation of average crystal sizes in **MOF-525** nanocrystals and **MOF-525**/GNRs nanocomposites from Fig. S3.

	Average crystal size (nm)	Standard deviation (nm)	Number of crystals counted
MOF-525 nanocrystals	220	71.4	20
MOF-GNRs-5	219	41.7	20
MOF-GNRs-10	170	36.0	20
MOF-GNRs-25	119	27.4	20
MOF-GNRs-50	88.0	22.1	20

S4. Additional SEM images of MOF-GNRs-50 and pristine GNRs

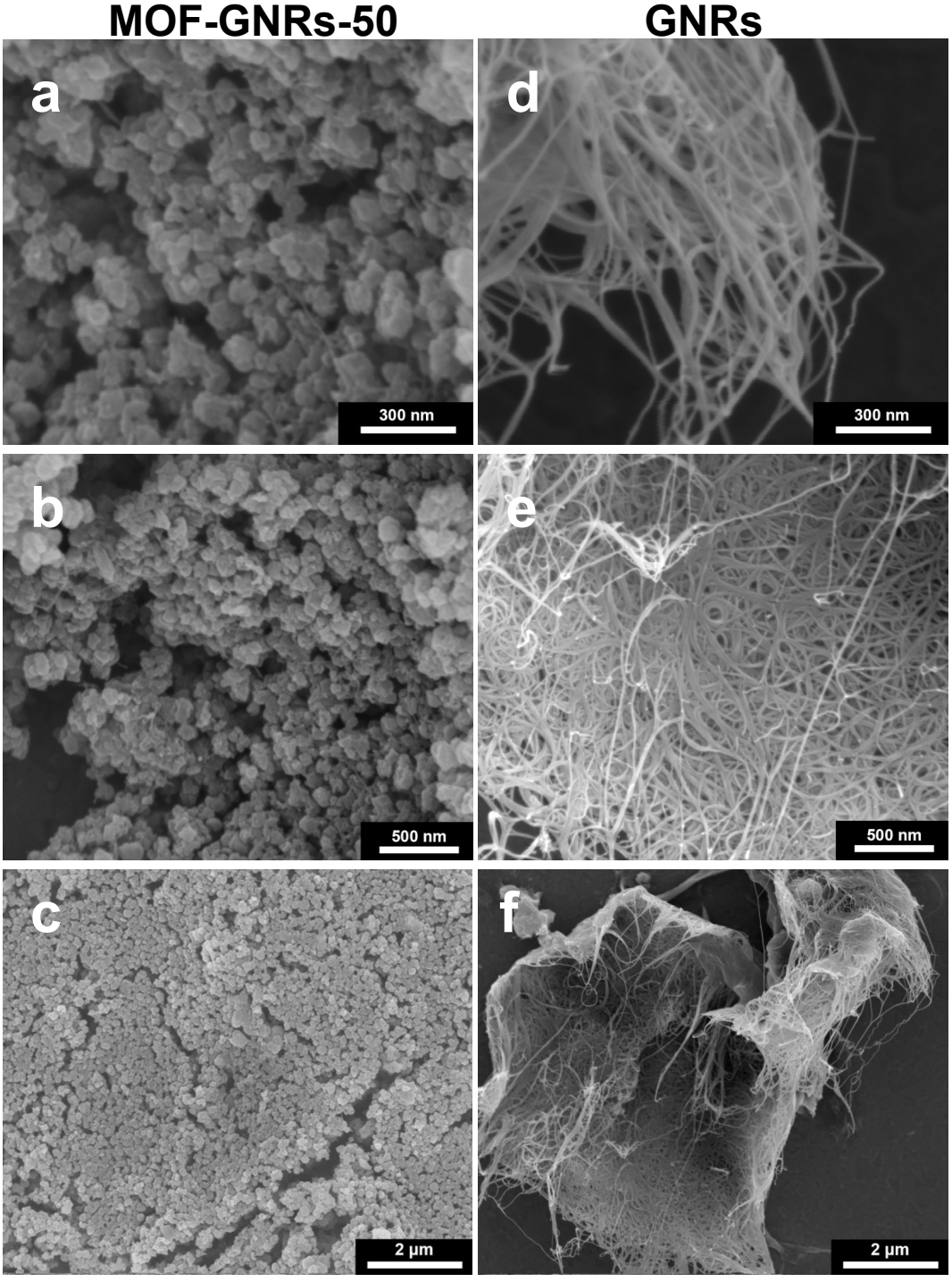

Figure S4. SEM images of MOF-GNRs-50 at a) high, b) mid, and c) low magnification. SEM images of pristine GNRs at d) high, e) mid, and f) low magnification.

S5. High-resolution TEM images of MOF-GNRs-50

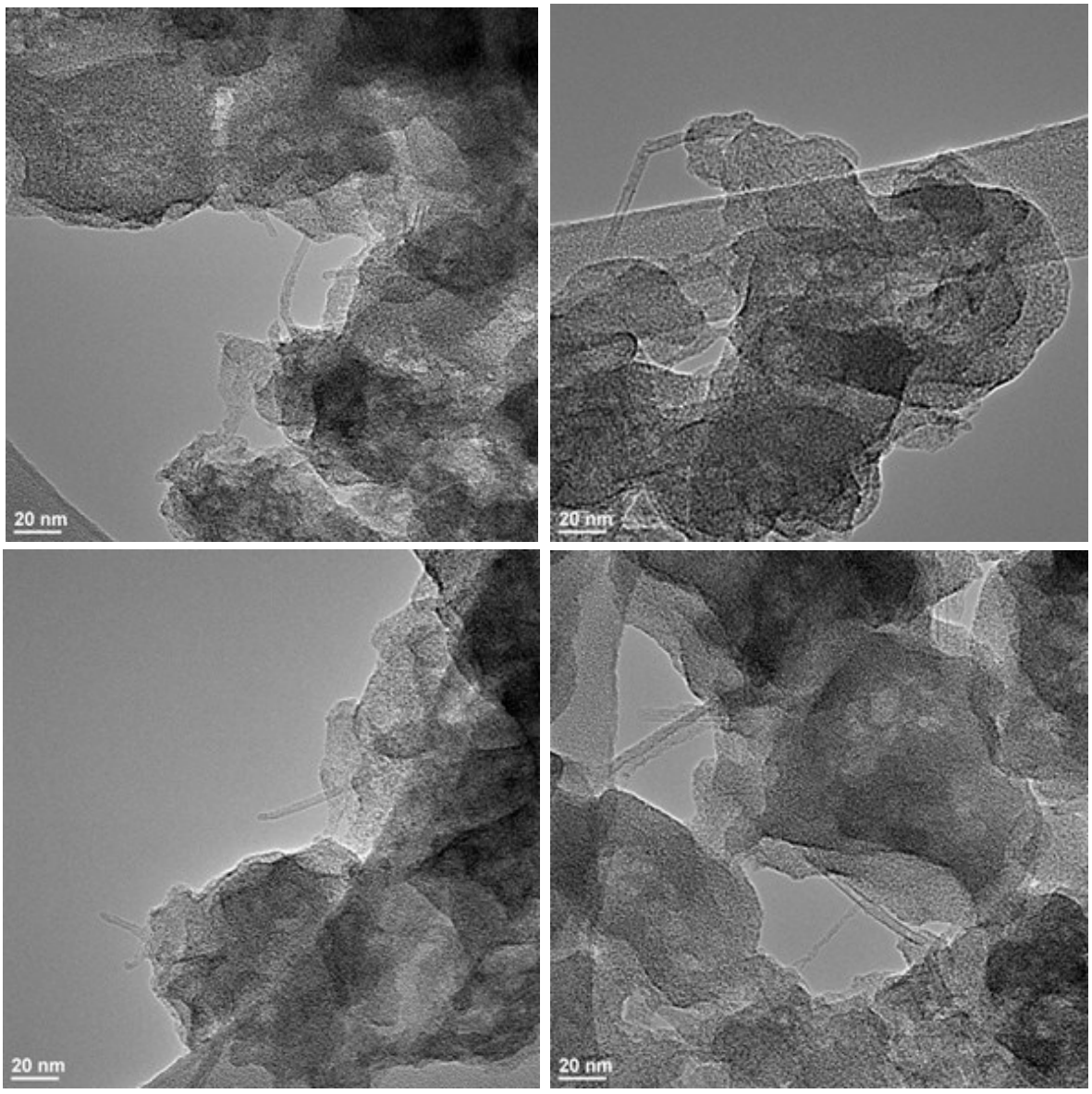

Figure S5. Four high-resolution TEM images of MOF-GNRs-50.

S6. XRD pattern of GNRs

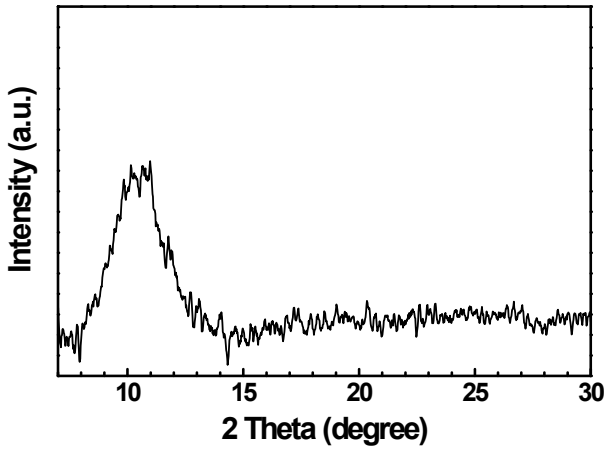

Figure S6. XRD pattern of GNRs.

S7. DFT pore size distribution

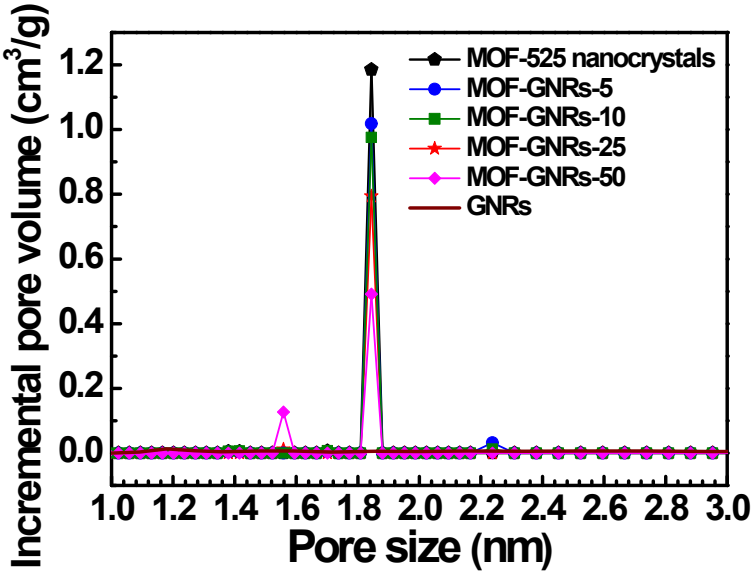

Figure S7. DFT pore size distributions of **MOF-525** nanocrystals, MOF/GNRs nanocomposites, and GNRs, calculated by using the cylindrical-pore model.

S8. Electrocatalytic nitrite oxidation on drop-cast thin films of MOF-525 nanocrystals

In order to select a proper experimental procedure for thin-film deposition, the suspensions of **MOF-525** nanocrystals with various concentrations, including 1, 2, 5, and 10 mg/mL, were prepared and used for drop casting. Uniform thin films of **MOF-525** can thus be obtained on ITO substrates. CV curves of the obtained thin films were measured in 0.1 M KCl aqueous solutions containing various concentrations of nitrite ranging from 0 to 0.75 mM; bare ITO substrate was also examined for comparison (see Fig. S8). It can be observed that the current density for nitrite oxidation measured on the bare ITO substrate (Fig. S8a) is nearly negligible compared to those measured on the thin films of **MOF-525** nanocrystals (Fig. S8b to Fig. S8e). In addition, from Fig. S8b to Fig. S8e, it can be seen that the catalytic current density increases with increasing concentration of suspension. The relationship between $\Delta J_{0.75\ \mathrm{mM}}$ measured at 0.9 V, which is defined as the difference in current density between the CV curves measured in the absence of nitrite and in 0.75 mM of nitrite, and the concentration of suspension used for thin-film deposition, is shown in Fig. S9. The spot at 0 mg/mL indicates the result of the bare ITO substrate. The effect of concentration of suspension used for drop casting can be clearly observed in Fig. S9. The thin film of **MOF-525** nanocrystals deposited by using 10 mg/mL of suspension achieves the highest catalytic current for nitrite, and it exhibits a stable electrochemical signal in 0.1 M KCl aqueous solution during cycling (Fig. S10). However, when a higher concentration, *i.e.*, 20 mg/mL, was used for drop casting, the obtained thin film cracked during drying. Therefore, 10 mg/mL of suspension was selected as the optimal concentration for the deposition of **MOF-525** thin film.

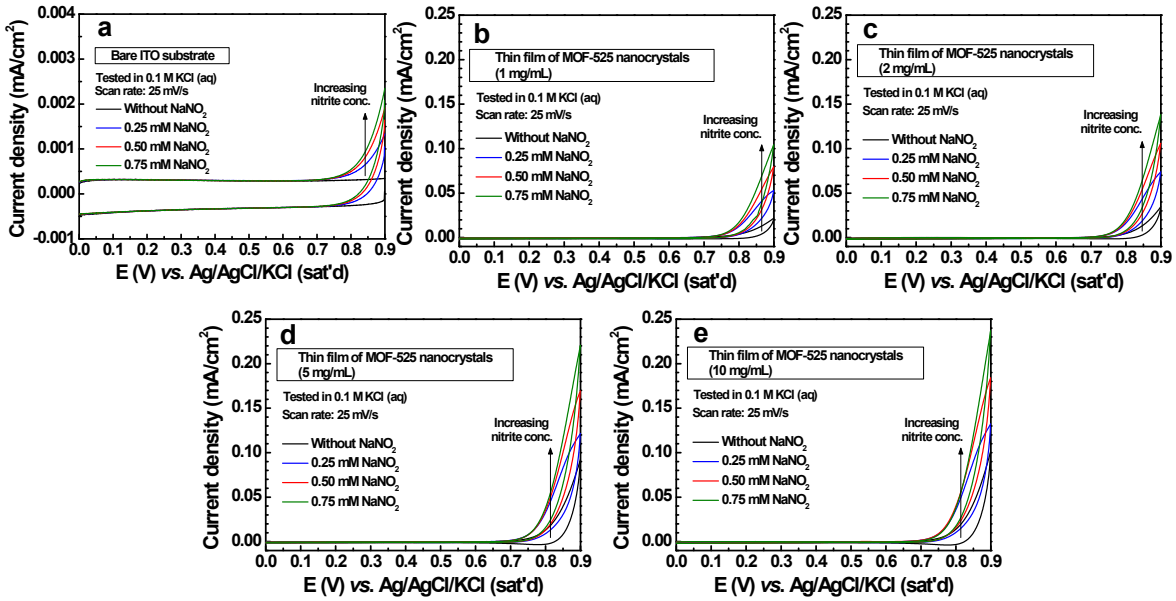

Figure S8. CV curves of a) bare ITO substrate and thin films of **MOF-525** nanocrystals deposited by using b) 1 mg/mL, c) 2 mg/mL, d) 5 mg/mL, and e) 10 mg/mL of suspensions, measured in 0.1 M KCl aqueous solutions containing 0, 0.25, 0.50, and 0.75 mM of nitrite.

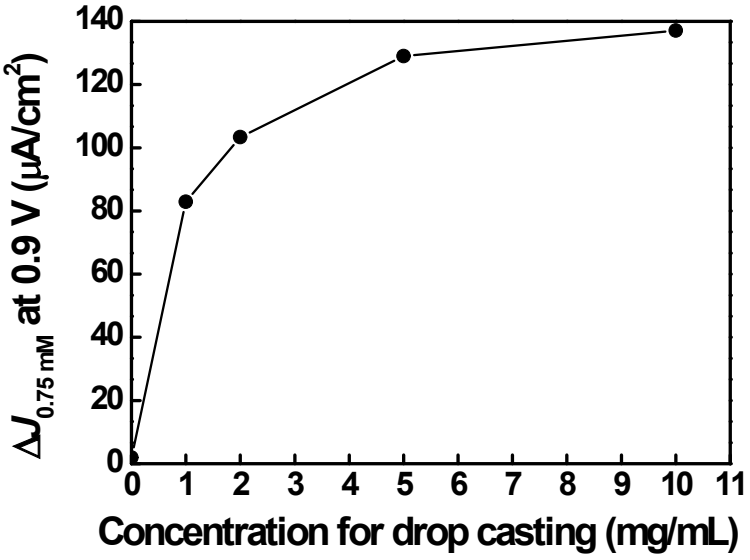

Figure S9. Relationship between $\Delta J_{0.75\ mM}$ measured at 0.9 V and the concentration of suspension used for thin-film deposition.

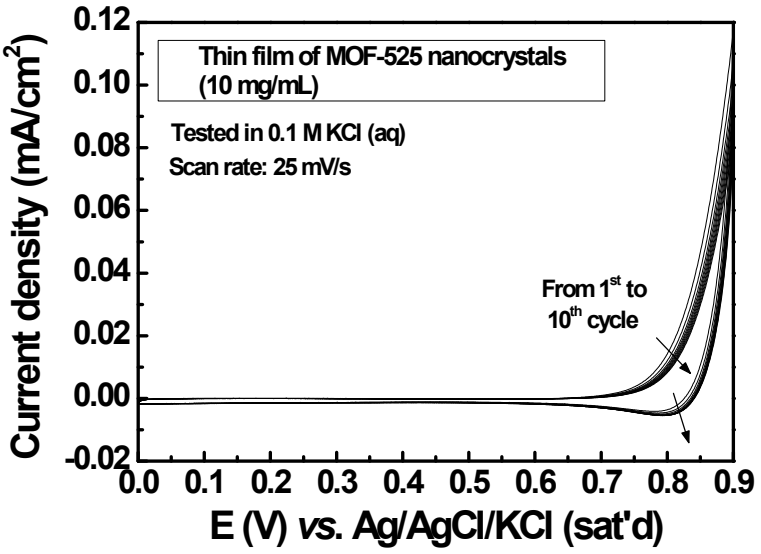

Figure S10. 10-cycle CV curve of the thin film of **MOF-525** nanocrystals deposited by using 10 mg/mL of suspension.

S9. Performance comparison

Table S2. Partial list of literatures reporting electrocatalytic nitrite oxidation under neutral pH and utilizing it for nitrite sensors.

Electrocatalyst	Performance			Potential vs. Ag/AgCl/KCl (sat'd)	Reference
	Sensitivity (μA/mM-cm^2)	LOD (μM)	Linear range (up to, μM)		
Pd/Fe alloy	23.3	0.8	25500	0.59	[S1]
Hemoglobin/Au NPs/graphene [a]	150	0.01	1000	0.9	[S2]
Hemoglobin/Au nanorods/graphene oxide	111	0.025	103	0.75	[S3]
Au NPs/Co(II)porphyrin	71	0.06	4700	0.9	[S4]
Cobalt phthalocyanine/graphene	74.3	0.084	36	0.85	[S5]
Cobalt phthalocyanine/MWCNTs [b]	421	0.062	340	0.85	[S6]
Au NPs/copper hydroxide	5383	0.5	191	0.81	[S7]
PEDOT nanorods [c]	321	0.57	40	0.82	[S8]
PEDOT/MWCNTs	140	0.96	1000	0.6	[S9]
Solvothermally grown **MOF-525** thin film	95	2.1	800	0.9	[S10]
MOF-GNRs-50 thin film	93.8	0.75	2500	0.85	This study

[a] NPs=nanoparticles

[b] MWCNTs=multiwalled carbon nanotubes

[c] PEDOT=poly(3,4-ethylenedioxythiophene)

S10. Reference

[S1] J. Wang, H. Zhou, D. Fan, D. Zhao and C. Xu, *Microchim. Acta*, 2015, **182**, 1055.

[S2] J. Jiang, W. Fan and X. Du, *Biosens. Bioelectron.*, 2014, **51**, 343.

[S3] C. Wang, X. Zou, Q. Wang, K. Shi, J. Tan, X. Zhao, Y. chai and R. Yuan, *Anal. Methods*, 2014, **6**, 758.

[S4] P. Muthukumar and S. A. John, *J. Colloid Interface Sci.*, 2014, **421**, 78.

[S5] L. Cui, T. Pu, Y. Liu and X. He, *Electrochim. Acta*, 2013, **88**, 559.

[S6] P. Li, Y. Ding, A. Wang, L. Zhou, S. Wei, Y. Zhou, Y. Tang, Y. Chen, C. Cai and T. Lu, *ACS Appl. Mater. Interfaces*, 2013, **5**, 2255.

[S7] L. Cui, X. M. Meng, M. R. Xu, K. Shang, S. Y. Ai and Y. P. Liu, *Electrochim. Acta*, 2011, **56**, 9769.

[S8] H. Mao, X. Liu, D. Chao, L. Cui, Y. Li, W. Zhang and C. Wang, *J. Mater. Chem.*, 2010, **20**, 10277.

[S9] C. Y. Lin, V. S. Vasantha and K. C. Ho, *Sens. Actuators B*, 2009, **140**, 51.

[S10] C. W. Kung, T. H. Chang, L. Y. Chou, J. T. Hupp, O. K. Farha and K. C. Ho, *Electrochem. Commun.*, 2015, **58**, 51.